Geophysical Research Letters

RESEARCH LETTER
10.1029/2019GL086631

El Niño-Driven Oxygenation Impacts Peruvian Shelf Iron Supply to the South Pacific Ocean

Insa Rapp[1,2], Christian Schlosser[1], Thomas J. Browning[1], Fabian Wolf[1,3], Frédéric A. C. Le Moigne[1,4], Martha Gledhill[1], and Eric P. Achterberg[1]

[1]Marine Biogeochemistry Division, GEOMAR Helmholtz Centre for Ocean Research Kiel, Kiel, Germany, [2]Now at Department of Biology, Dalhousie University, Halifax, Nova Scotia, Canada, [3]Now at Marine Ecology Division, GEOMAR Helmholtz Centre for Ocean Research Kiel, Kiel, Germany, [4]Now at Mediterranean Institute of Oceanography, Marseille, France

Key Points:
- Redox state and trace element measurements were performed on a set of across shelf transects in the Peruvian OMZ during the 2015 El Niño
- El Niño oxygenation of the North Peruvian shelf resulted in decreased water column inventories of redox-sensitive trace metals Fe, Co, and Mn
- Resulting increases in N:Fe supply ratios to surface waters may have led to faster offshore transitions to Fe limited phytoplankton growth

Supporting Information:
- Supporting Information S1

Correspondence to:
I. Rapp and E. P. Achterberg,
irapp@geomar.de

Citation:
Rapp, I., Schlosser, C., Browning, T. J., Wolf, F., Le Moigne, F. A. C., Gledhill, M., & Achterberg, E. P. (2020). El Niño-driven oxygenation impacts Peruvian shelf iron supply to the South Pacific Ocean. *Geophysical Research Letters*, *46*. https://doi.org/10.1029/2019GL086631

Received 20 DEC 2019
Accepted 11 MAR 2020
Accepted article online 13 MAR 2020

© 2020. The Authors.
This is an open access article under the terms of the Creative Commons Attribution License, which permits use, distribution and reproduction in any medium, provided the original work is properly cited.

Abstract Upwelling ocean currents associated with oxygen minimum zones (OMZs) supply nutrients fuelling intense marine productivity. Perturbations in the extent and intensity of OMZs are projected in the future, but it is currently uncertain how this will impact fluxes of redox-sensitive trace metal micronutrients to the surface ocean. Here we report seawater concentrations of Fe, Mn, Co, Cd, and Ni alongside the redox indicator iodide/iodate in the Peruvian OMZ during the 2015 El Niño event. The El Niño drove atypical upwelling of oxygen-enriched water over the Peruvian Shelf, resulting in oxidized iodine and strongly depleted Fe (II), total dissolved Fe, and reactive particulate Fe concentrations relative to non-El Niño conditions. Observations of Fe were matched by the redox-sensitive micronutrients Co and Mn, but not by non-redox-sensitive Cd and Ni. These observations demonstrate that oxygenation of OMZs significantly reduces water column inventories of redox-sensitive micronutrients, with potential impacts on ocean productivity.

Plain Language Summary Some trace metals, including iron, are essential micronutrients for phytoplankton growth. However, the solubility of iron is very low under oxygenated conditions. Consequently, restricted iron availability in oxygen-rich seawater can limit phytoplankton growth in the ocean, including in the Eastern Tropical South Pacific. Under typical conditions, depleted oxygen on the South American continental shelf is generally thought to enhance iron supply to the ocean, fuelling phytoplankton productivity in overlying waters. However, the impacts of changes in oxygenation, which are predicted to occur in the future, are not known. The 2015 El Niño event led to unusually high oxygen on the Peruvian shelf, offering a system-scale test on how oxygen influences seawater iron concentrations. We show that El Niño-driven oxygenation resulted in marked decreases in iron and other metals sensitive to oxygen (cobalt and manganese), while metals not sensitive to oxygen (cadmium and nickel) were unaffected. The measured reductions in iron may have led to decreased phytoplankton productivity.

1. Introduction

Coastal waters associated with eastern boundary currents receive high inputs of macronutrients (N, P, and Si) and bioessential trace elements (Fe, Mn, Co, Zn, and Cd) as deeper waters upwell to the surface (Bruland et al., 2005; Lohan & Bruland, 2008). Consequently, phytoplankton productivity in these regions is among the highest globally (Carr, 2001), which in turn reduces the fugacity of upwelled CO_2 and sustains up to 20% of global fish catch (Pauly & Christensen, 1995). However, taking into account phytoplankton requirements, upwelled waters are deficient in Fe relative to macronutrients (Bruland et al., 2005; Moore et al., 2013). Therefore, during off shelf transport of surface waters, phytoplankton growth can deplete Fe to limiting levels, leading to sharp reductions in phytoplankton productivity (Browning et al., 2017, 2018; Hutchins et al., 2002; Moore et al., 2013). Further offshore, concentrations of both Fe and macronutrients are depleted (Noble et al., 2012) and can colimit growth (Bonnet et al., 2008; Browning et al., 2017; Ward et al., 2013). Constraining the factors that determine Fe supply in eastern boundary currents is therefore critical for projecting biogeochemical feedback to physical-chemical perturbations in these systems (Capone & Hutchins, 2013).

The Peruvian shelf in the eastern tropical South Pacific is one such coastal upwelling system, which itself alone accounts for ~10% of global fish landings (Christensen et al., 2014). This region is part of a large

oxygen minimum zone (OMZ) where oxygen-depleted bottom waters (<5 μM O_2 over ~100- to 500-m water depth; Karstensen et al., 2008) typically lead to very high benthic Fe fluxes (up to ~300 mmol · m^{-1} · $year^{-1}$; Noffke et al., 2012) that constitute the dominant Fe source to surface waters (Chever et al., 2015), whereas atmospheric Fe inputs are relatively minor (Buck et al., 2019). These enhanced benthic fluxes are driven by diagenetic processes in anoxic sediment pore waters that reduce particulate Fe (III) species to soluble Fe (II), which is subsequently released into overlying bottom waters by diffusion, pore water efflux, and sediment resuspension (Burdige, 1993; Chaillou et al., 2002; Froelich et al., 1979). Fe (II) is rapidly oxidized in the presence of oxygen (Millero et al., 1987) and potentially also in the absence of oxygen by Fe (II)-oxidizing microbial nitrate reduction (Heller et al., 2017; Scholz et al., 2016). This process results in the formation of particulate Fe with subsequent removal via precipitation, whereas a portion of the oxidized Fe may stay in solution via stabilization by organic ligands (Gledhill & Buck, 2012) and formation of small slow sinking colloidal particles (Lam et al., 2012). Conversely, particularly high bottom water dFe concentrations (up to 300 nM) under sulfidic conditions indicate Fe (II) being stable in the absence of both oxygen and nitrate/nitrite (Schlosser et al., 2018; Scholz et al., 2016). Despite the presence of oxidation mechanisms, the combination of a strong sedimentary source and slow oxidation kinetics under low oxygen conditions typically lead to elevated dissolved Fe (dFe) concentrations within OMZ waters over the Peruvian shelf (from a few nM up to ~80 nM under nonsulfidic conditions; Bruland et al., 2005; Chever et al., 2015; Vedamati et al., 2014).

Cobalt and Mn are other redox-sensitive micronutrient trace metals (TMs) that exhibit increased water column concentrations under low oxygen conditions, likely due to enhanced release from sediments and slow oxidation kinetics (Hawco et al., 2016; Noble et al., 2012; Rapp et al., 2019). In contrast, the nonredox sensitive TMs Cd and Ni show oceanic vertical profiles that are strongly regulated by biological uptake and remineralization (Bruland & Lohan, 2006). Cadmium and Ni are also released into benthic pore waters during organic matter remineralization, but their sediment fluxes are usually low, with only slightly higher pore water concentrations compared to bottom water levels (Biller & Bruland, 2013; Klinkhammer et al., 1982). Conversely, the presence of H_2S in sediments and water column can lead to removal of Cd and Ni through formation of solid sulfide minerals, whereas the formation of solid Fe sulfides is unlikely to occur at typical seawater concentrations of Fe and H_2S in our study region due to the higher solubility of Fe sulfides (Plass et al., 2019; Schlosser et al., 2018).

The complexity of processes regulating benthic Fe release, water column Fe removal, and dynamics of offshore transport in OMZs means that current projections of net changes in water column Fe concentrations with modified future oxygen levels (Schmidtko et al., 2017) are highly uncertain. We measured seawater concentrations of Fe (II), dFe, and reactive particulate Fe together with other bioessential redox-sensitive (Co and Mn) and non-redox-sensitive (Ni and Cd) TMs in the Peruvian OMZ, which experienced changes in water column oxygenation state as a result of a strong 2015/2016 El Niño event (Stramma et al., 2016) and thereby offered a realistic system-scale test on the sensitivity of these elements to changes in seawater oxygenation state. As Fe is a limiting nutrient in this region (Browning et al., 2018), we focused on this element and used concentrations of additional TMs (Co, Mn, Ni, and Cd) as tools to separate redox-driven changes in Fe distribution from changes in other sources, such as remineralization and deep water upwelling.

2. Material and Methods

Samples were collected on *RV Sonne* cruise SO243 (8–19 October 2015) at 12 stations on four cross-shelf transects off the Peruvian coast between 9 and 17°S. In October 2015 the sea surface temperature anomaly was > +2.0 °C near the equator (for definition see Text S1 in the supporting information) and therefore considered a strong El Niño (National Oceanic and Atmospheric Administration, 2017; Stramma et al., 2016). Sea surface temperature anomalies above +0.5 °C prevailed between March 2015 and June 2016 and peaked from November 2015 and to January 2016 (National Oceanic and Atmospheric Administration, 2017).

Samples for TMs and iodide/iodate were collected following GEOTRACES protocols using Ocean Test Equipment samplers deployed on a Kevlar wire (Cutter et al., 2010). TM samples were collected in acid-cleaned low-density polyethylene bottles (Nalgene), either unfiltered (total dissolvable [TD] TMs) or filtered (0.2-μm AcroPak 500 cartridge filters, Pall; dissolved TMs). Samples were acidified to pH ~1.9 by

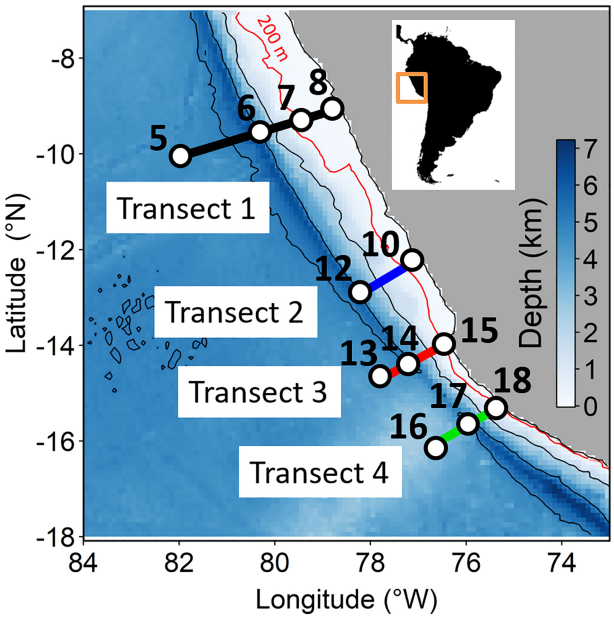

Figure 1. Map of sampling sites along the four cross-shelf transects. The blue color shading indicates bathymetry, with decreasing shelf width in the north to south direction as highlighted by red bathymetry line for 200-m depth.

adding 150-μl ultrapure HCl (OPTIMA grade, Fisher Scientific) per 125-ml sample and stored double-bagged for >6 months. Samples for Fe (II) determination were collected unfiltered in acid-cleaned opaque high-density polyethylene bottles (Nalgene) and immediately analyzed on-board using luminol chemiluminescence flow injection analysis without preconcentration (Hopwood et al., 2017; SI Text S2). Samples for iodide and iodate measurements were filtered (0.2-μm AcroPak 500 cartridge filter), collected in opaque high-density polyethylene bottles (Nalgene), and stored frozen at −20 °C until analysis.

Dissolved (d) and TD TM samples were preconcentrated and analyzed for Fe, Co, Mn, Cd, Ni, Pb, Zn, and Cu, with preconcentration and matrix removal using an automated device (SeaFAST, Elemental Scientific Inc. [ESI]) equipped with a cation exchange resin (WAKO; Kagaya et al., 2009) and analysis by high-resolution inductively coupled plasma-mass spectrometry (Element XR, Thermo Fisher Scientific; Rapp et al., 2017, and Text S3). Here we only show data for Fe, Co, Mn, Cd, and Ni. The data of all analyzed TMs are available in the available data file (see data availability statement). The concentration of reactive particulate (reactive p) TMs was in this study defined as the difference between TD and dissolved TM concentrations. Uncertainties on the TM measurements calculated using the Nordtest approach (Näykki et al., 2015; Rapp et al., 2017) were 22% for Fe (excluding Fe (II)), 11% for Ni, 23% for Co, 17% for Mn, and 13% for Cd. The standard deviation for reactive pFe was determined as combined error of dFe and TDFe and ranged between 22 and 33%.

Both redox species of iodine have limited particle reactivity and thereby stay in solution, resulting in relatively high concentrations that can be accurately quantified (total iodine ~500 nM; Wong & Brewer, 1977). Iodide/iodate samples were defrosted overnight at room temperature and analyzed for iodide by cathodic stripping square wave voltammetry (Luther et al., 1988), and stored refrigerated for a maximum of 5 days until iodate analysis. Iodate concentrations were analyzed spectrophotometrically at room temperature following sulfamic acid reduction (Chapman & Liss, 1977).

Macronutrients were sampled using a stainless steel CTD-rosette package (Stramma et al., 2016). On-board nutrient measurements of nitrite (NO_2^-), nitrate (NO_3^-), phosphate (PO_4^{3-}), and silicic acid ($Si(OH)_4$) were conducted using a QuAAtro autoanalyzer (Seal Analytical). Oxygen, temperature, and conductivity were measured with double sensors by the CTD. Oxygen concentrations of discrete water samples (Winkler titration) were used to calibrate the CTD oxygen sensor.

3. Results and Discussion

3.1. El Niño Modified Water Column

Seawater samples were collected on a cruise that traversed the Peruvian shelf in October 2015 (Figure 1), which was during the strong 2015/2016 El Niño event (Stramma et al., 2016). Four cross-shelf transects along the Peruvian coast from 9 to 16°S exhibited different magnitudes of El Niño-induced water column oxygenation (Figures 2b, 3b, and S1 in the supporting information). El Niño induced upwelling of atypical warmer, lighter, and relatively oxygen-rich waters over Transect 1 occupying the North Peru shelf, with lowest oxygen values only observed in deeper waters (4–5 μM O_2 at 240- to 600-m depth; Figures 3 and S1; Stramma et al., 2016). At oxygen concentrations below the detection limit for conventional methods (~2–3 μM O_2), the redox-couple iodate (IO_3^-) and iodide (I^-) is a useful indicator for suboxic conditions as iodine (I) is one of the first elements that undergoes reduction upon oxygen depletion (redox sequence: oxygen > iodate > nitrate > Fe (III) > sulfate; Cutter et al., 2018). In addition to the reduction of iodate to iodide under suboxic conditions, iodide is produced in oxygenated surface waters, likely during photosynthesis (Wong et al., 2002). Along Transect 1, full reduction of I occurred only within a narrow zone around 400-m depth as indicated by ratios of reduced iodine (iodide) to total inorganic iodine (iodide + iodate) close to 1 (Figure 3c). In contrast, the three transects to the south (Transects 2–4) were characterized by sharp,

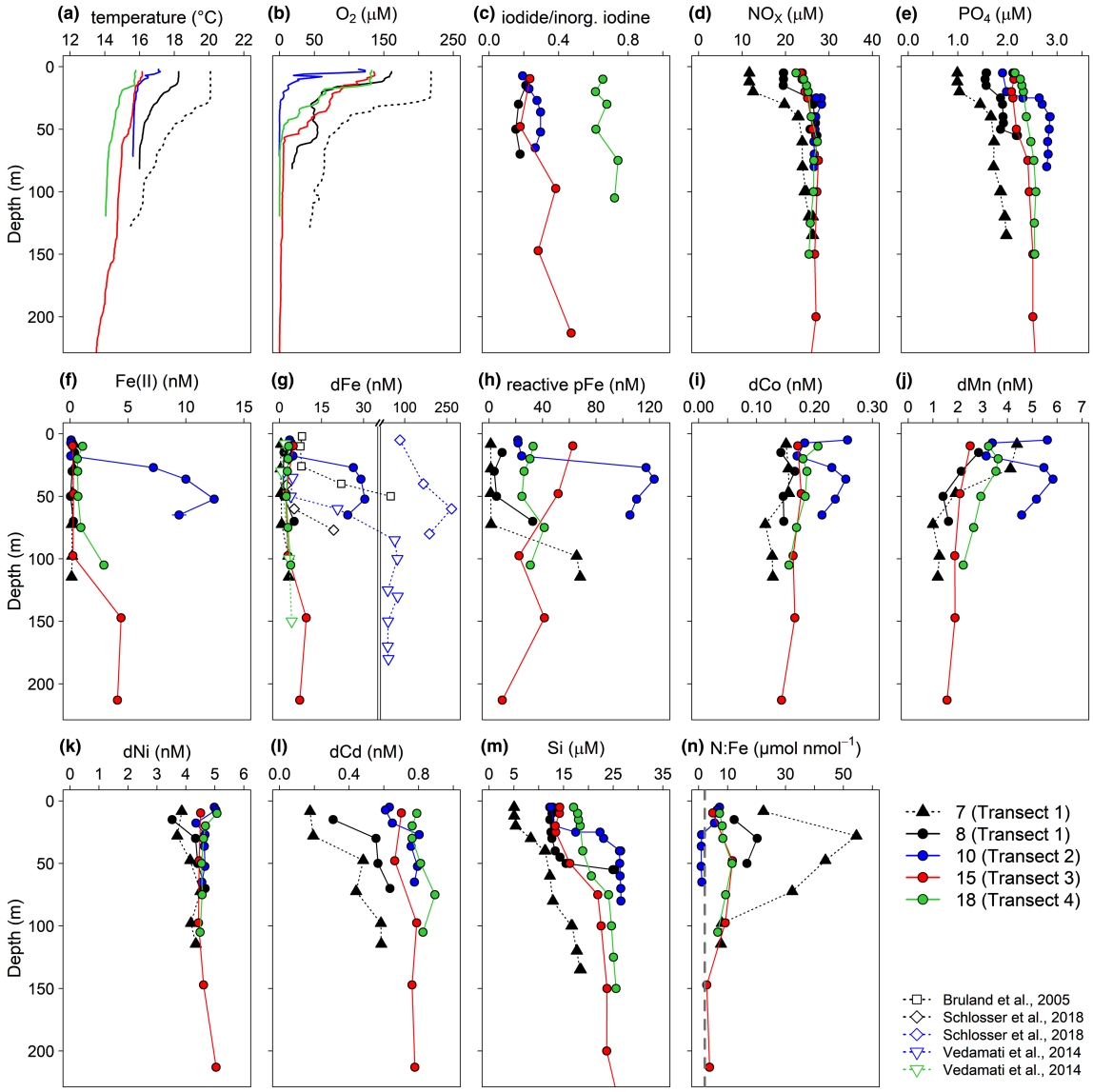

Figure 2. Onshore variability in trace metal and nutrient distributions. Temperature, oxygen, iodine to total inorganic iodine ratios, nitrate + nitrite (NO_X), phosphate (PO_4), Fe (II), dFe, and reactive pFe fractions; dissolved trace metals (dCo, dMn, dNi, and dCd); silicic acid (Si); and N:Fe depth profiles of five onshore stations. Additional literature data of dFe from stations close to our transect locations are shown (g). The vertical dashed line (n) shows assumed average phytoplankton N:Fe (from synthesis values in Moore et al., 2013).

shallow oxyclines ($O_2 < 5$ μM below 50 m) and upwelling of cold, oxygen-depleted, macronutrient-enriched waters over the shelf, which is typical of non-El Niño conditions (Stramma et al., 2016). Near-complete iodine reduction was also found over a broader and shallower depth range in the more southerly transects (200–400 m at Transects 2 and 3, and 150–400 m at Transect 4; Figures 3c and S1).

3.2. Trace Metal Distributions

Three fractions of water column Fe concentrations were determined on the cruise transects comprising reduced Fe (II), dFe (Fe (II) + Fe (III)), and reactive particulate Fe (reactive pFe). All Fe fractions for all four transects (with the exception of Fe (II) at Transect 1) showed enhanced concentrations over the shelf and a decrease beyond the shelf break (Figures 2f–2h, 3f–3h, and S1)—consistent with studies reporting strong removal of benthic-derived Fe during offshore transport (Bruland et al., 2005; Vedamati et al., 2014). An additional observation common to all transects was the presence of elevated dFe and reactive pFe at the upper part of the OMZ from 100 to 300 m (density anomalies of 26.0–26.5 kg/m^3; Figures 3g and 3h and

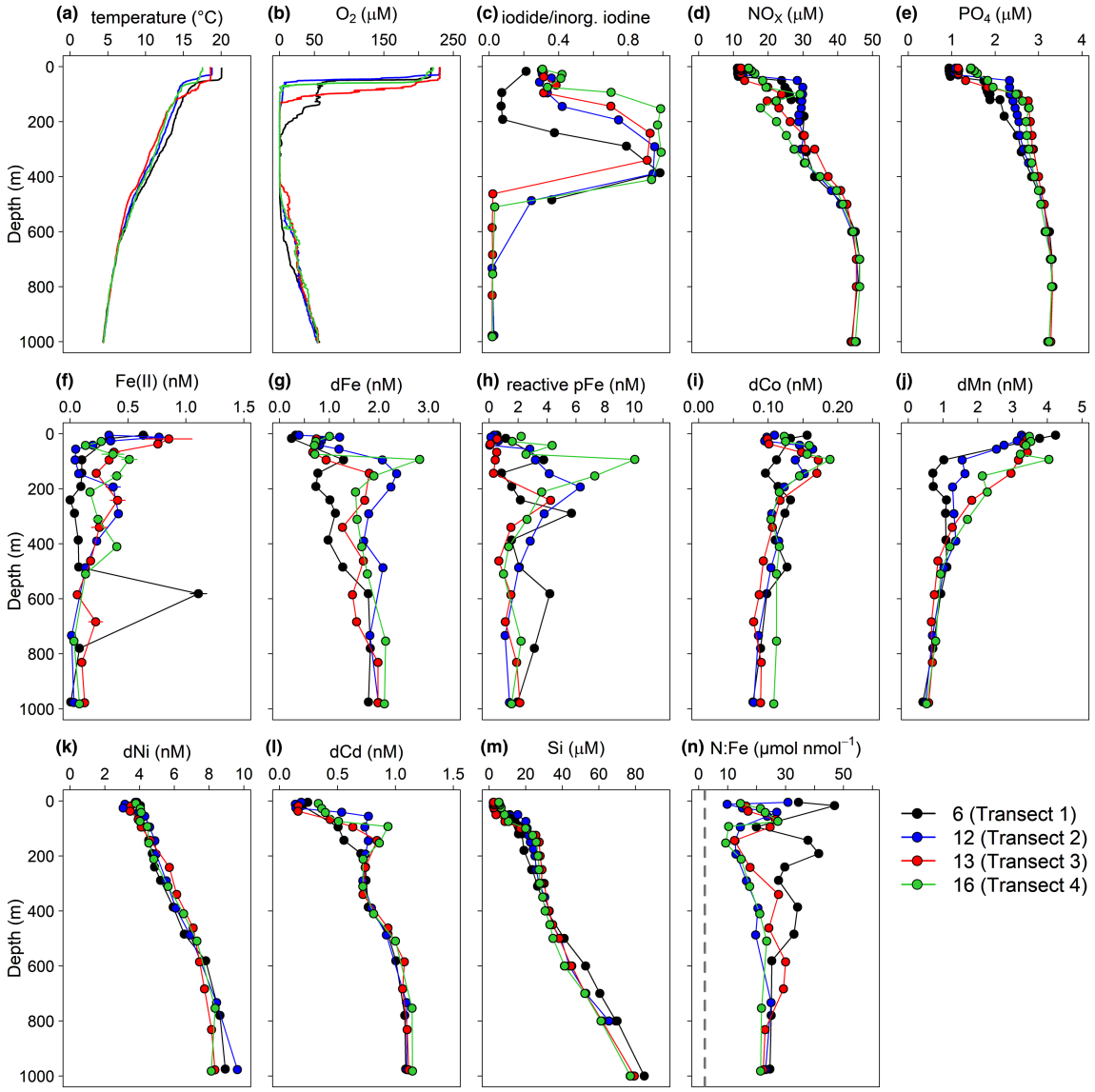

Figure 3. Offshore variability in trace metal and nutrient distributions. Temperature, oxygen, iodine to total inorganic iodine ratios, nitrate + nitrite (NO_x), phosphate (PO_4), Fe (II), dFe, and reactive pFe fractions; dissolved trace metals (dCo, dMn, dNi, and dCd); silicic acid (Si); and N:Fe depth profiles of four offshore stations with similar distance from the coast (130–170 km). The vertical dashed line (n) shows assumed average phytoplankton N:Fe (from synthesis values in Moore et al., 2013).

4a and 4b). This feature has been previously documented for dFe, particulate Fe, and Fe (II) in the region and was related to a laterally transported shelf source (Cutter et al., 2018; Heller et al., 2017). In our study we also found that concentrations of other redox-sensitive TMs, dCo and dMn, were elevated in this part of the water column, while non-redox-sensitive TMs dCd and dNi remained unchanged, instead exhibiting profiles resembling macronutrients (Figures 3 and 4). In contrast to Fe, neither reactive pMn nor reactive pCo showed clear increases between 100 and 300 m (data not shown), potentially because these pools constituted smaller fractions of TD concentrations (0–45% reactive pCo/TDCo and 0–36% reactive pMn/TDMn cf. 9–95% reactive pFe/TDFe).

Part of the reactive pFe maxima in the upper OMZ may have formed in situ, by two mechanisms: adsorption of dFe onto particle surfaces and/or oxidation of Fe (II) to amorphous Fe (oxyhydr)oxides by traces of oxygen, hydrogen peroxide, or in connection with microbial nitrate reduction (Heller et al., 2017). Enhanced concentrations of Fe, Co, and Mn in this density layer alongside the absence of this feature for Ni, Cd, silicic acid, and PO_4 (Figure 4) point toward a dominant role of elevated benthic release on the shelf at shallower

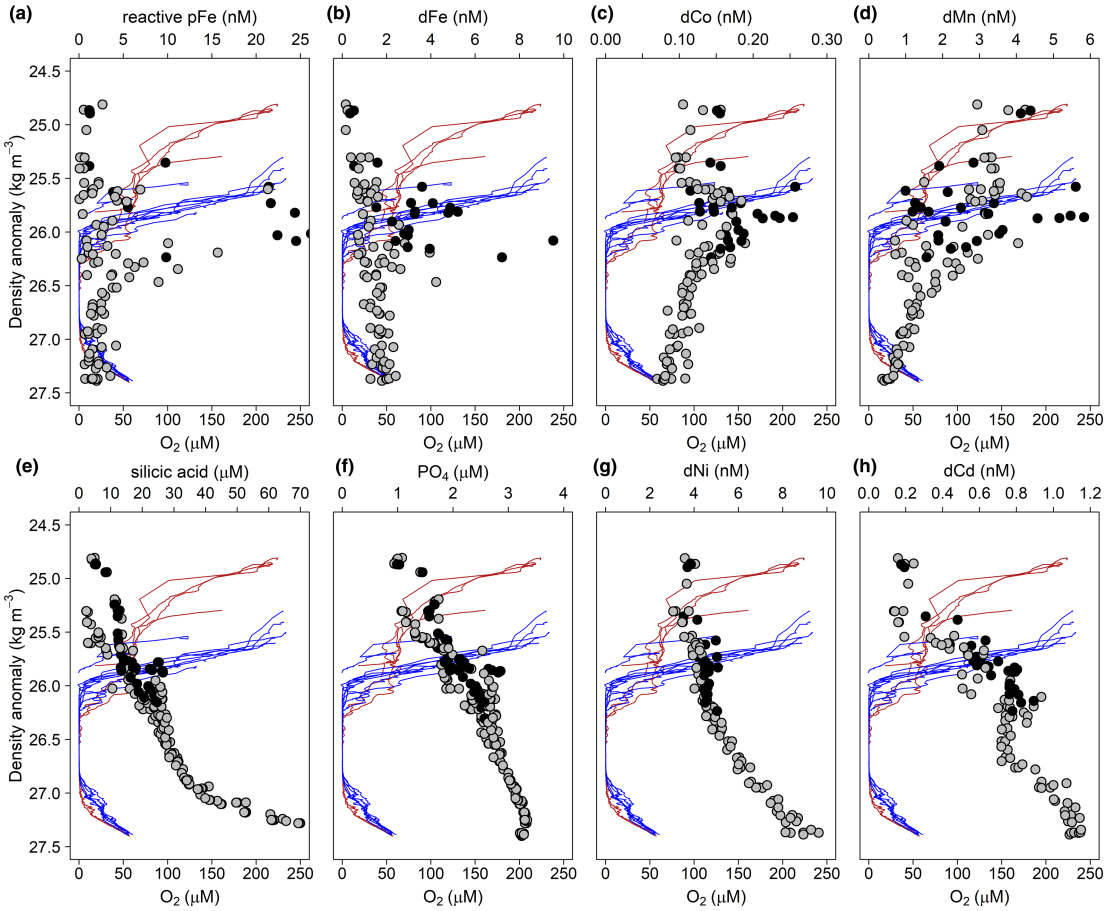

Figure 4. Oxygen, trace metals, and macronutrient density distributions. Data from all stations are shown: the gray and black dots indicate trace metal or macronutrient concentrations at offshore (bottom depth > 2,000 m) and onshore (bottom depth < 300 m) stations, respectively. The lines indicate oxygen concentrations from Transect 1 (red) and Transects 2–4 (blue). Highest Fe concentrations at onshore stations for Transects 1–3 exceed the scale (up to 124-nM reactive pFe and 30.4-nM dFe).

OMZ depths followed by offshore transport (Noble et al., 2012; Noffke et al., 2012) rather than enhanced input through remineralization. A common source for Fe, Mn, and Co was supported by a strong correlation between dCo and dMn ($R^2 = 0.80$: $p = 2.2 \times 10^{-16}$) in the density layer 25.7–26.5 kg/m^3 and moderate correlations between dFe and dCo ($R^2 = 0.48$: $p = 2.5 \times 10^{-8}$) and dFe and dMn ($R^2 = 0.50$: $p = 7.6 \times 10^{-9}$; Figure S2). The weaker correlations of dMn and dCo with dFe are probably a result of a faster removal of dFe compared to dCo and dMn in the presence of oxygen (Noble et al., 2012). Increased activities of benthic-derived ^{228}Ra, which indicate relatively recent contact with the shelf (^{228}Ra half-life 5.75 yr), have been observed in the Peruvian upwelling system within the upper 200 m relative to greater depths (Sanial et al., 2018), supporting this interpretation. Furthermore, enhanced calculated "excess iodide" (SI Text S4) at offshore sites, which is assumed to be sediment-derived (Cutter et al., 2018), matched peaks in redox-sensitive metals suggesting their sedimentary origin (Figure S3). Collectively these observations point toward the highest net flux of benthic-derived TMs at the top of the OMZ, where dissolved redox-sensitive TM concentrations are subsequently stabilized by lower oxygen concentrations (compared to shallower waters where increased removal by oxidation and microbial uptake occurs: Boyd & Ellwood, 2010; Lohan & Bruland, 2008). Enhanced surface water concentrations were only found for Mn, which is due to sustained photoreduction of insoluble Mn (IV) to soluble Mn (II) (Sunda & Huntsman, 1994).

3.3. Controls on Shelf Trace Metal Supply

The upwelled flux of Fe over coastal shelves is strongly influenced by both shelf width and the redox state of overlying waters (Bruland et al., 2001, 2005; Lohan & Bruland, 2008; Pakhomova et al., 2007; Severmann

et al., 2010); however, the relative influence of these two factors is not well constrained. Our cross-shelf transects occupied a southward decline in shelf width (defined here as the 200-m bottom depth contour) from ~95 km at 9°S to 30 km at 12°S, 13 km at 14°S, and 5 km at 15.5°S (Figure 1), while the prevalent El Niño conditions induced a reverse gradient in deoxygenation (Figure 2). This allows us to evaluate the relative importance of these two controls on Fe distributions in this system. Despite showing similar on-shelf to off-shelf trends, absolute concentrations of all Fe fractions showed substantial variability between the four cross-shelf transects, and this variability corresponded to seawater oxygenation state and oxycline depth (Figures 2 and 3). Lowest on-shelf Fe concentrations were found over the widest portion of the Peruvian shelf along Transect 1, where, uncharacteristically for the region, bottom water oxygen concentrations did not drop below 18 μM (with Fe (II) <0.29 nM close to sediments, dFe <5.2 nM, and reactive pFe <32.6 nM; Figures 2f–2h; Bruland et al., 2005). Highest on-shelf concentrations of all Fe fractions were found along Transect 2, where oxygen concentrations were <3 μM below 26 m (maximum Fe concentrations of 12.4 nM Fe (II) [52 m], 30.4 nM dFe [52 m], and 124 nM reactive pFe [36 m]). Between Transects 2 and 4, on-shelf concentrations of Fe (II), dFe and reactive pFe all decreased southward with declining shelf width, to maximum values of 2.9 nM Fe (II), 3.9 nM dFe, and 41.3 nM reactive pFe along Transect 4.

Moreover, in addition to overall concentrations, the contribution of the reduced—and most soluble—Fe (II) species to dFe (which includes Fe (II), complexed Fe (III), and colloidal Fe) close to the seafloor was much lower over the shelf in the north (Fe (II):dFe = 0.06 at Transect 1) relative to the three transects to the south, with progressively increasing contributions upon transitioning into more reducing conditions (Fe (II):dFe of 0.41, 0.57, and 0.74 for Transects 2, 3, and 4, respectively). While bottom water oxygen concentrations at Transects 2, 3, and 4 were all below detection limit (<3 μM) and therefore could not be used as an indicator for more subtle changes in redox status, ratios of iodide:total inorganic iodine revealed a shift to more reducing conditions between Transects 2 and 4 that correlated with Fe (II):dFe ratios (iodide:(iodide + iodate) of 0.26, 0.47, and 0.72 for Transects 2, 3, and 4, respectively; Figure S4). The contribution, and thereby the stability, of the most soluble Fe (II) species therefore appeared enhanced by more reducing conditions existing below the detection limit of oxygen concentrations.

The coastal distribution of Fe concentrations along the four cross shelf transects contrasts with previous studies in coastal upwelling sites with associated OMZs. Specifically, previous studies have reported highest Fe concentrations over the widest portions of continental shelves and shelf width has accordingly been interpreted as a dominant control on Fe fluxes to the water column (Bruland et al., 2001, 2005). For the widest section of the Peruvian shelf (Transect 1), we observed dFe concentrations that were ~10 times lower than previously reported values of ~50 nM at almost exactly the same location (9°S, 52-m water depth) under anoxic conditions (~0% oxygen saturation) and ~6 times lower than the ~30 nM reported slightly further south (10°S, 110-m water depth, O_2 ~0 μM), both measured during La Niña events (Bruland et al., 2005; Schlosser et al., 2018). At ~12°S, the approximate location of Transect 2, we measured dFe concentrations 2.5–10 times lower than the previously reported 75-nM dFe (neutral ENSO; O_2 < 5 μM; Vedamati et al., 2014) and 200- to 300-nM dFe (sulfidic conditions, neutral ENSO and La Niña; Schlosser et al., 2018; Scholz et al., 2016). In the southern part of the study region concentrations were similar to reported near-bottom dFe concentrations of 1.4–4.3 nM at 15–18°S during La Niña (Bruland et al., 2005) and neutral ENSO (Vedamati et al., 2014).

Despite a wider shelf at the site of Transect 1, previously reported dFe concentrations along Transect 2 were higher (Bruland et al., 2005; Schlosser et al., 2018; Scholz et al., 2016; Vedamati et al., 2014). This may be a result of consistently stronger sediment release at this part of the shelf, for example, via enhanced sediment resuspension driven by more active bottom water currents and waves (Homoky et al., 2016). Alongside the potential role of other factors, such variability in sediment resuspension occurring over the shelf may drive differences in water column Fe concentrations between El Niño and non-El Niño states. Our observations, however, argue against an isolated role of sediment resuspension between these two states and moreover indicate the importance of changes in Fe solubility: In addition to strong decreases in dFe compared to previous observations, enhanced El Niño-related oxygen concentrations in the water column of the Northern Peruvian Shelf decreased the more soluble Fe (II) fraction of dFe. Previous studies reported non-El Niño Fe (II) to dFe ratios of around 1 in bottom water at 12.36°S (Schlosser et al., 2018), at three locations between 12 and 16°S (Vedamati et al., 2014), and also slightly further north at around 6°S (Chever et al., 2015). This

was larger than any of our observed ratios (the maximum bottom water Fe (II):dFe ratio measured in this study was 0.74) particularly along Transect 1, which experienced the strongest influence of El Niño (Fe (II):dFe = 0.06). Such an El Niño shift in redox-state to a lower fraction of dFe present in the reduced form Fe (II) directly supports an influence of enhanced oxygen concentrations on dFe via a reduction in solubility. Collectively, these trends can be attributed to the strong influence of the prevailing oxidizing conditions over the northern Peruvian shelf under El Niño during our occupation, reflecting the net effect of diminished sedimentary Fe efflux and retention in the overlying water column despite hosting the widest surface area of shelf sediment for release to occur.

The distribution of other TMs supported the observed El Niño redox control of dFe. As for Fe, the redox-sensitive micronutrients dCo and dMn displayed lowest concentrations along the northern Transect 1 (Figures 2i and 2j), whereas concentrations of dCd showed a general increase in concentration with increasing density (Figure S5). The latter is consistent with remineralization control at individual stations and a shift to generally higher concentrations at more southerly stations with stronger upwelling of deeper (denser) waters hosting enhanced dCd.

3.4. Influence of El Niño on Offshore Trace Metal Distributions

The influence of El Niño on the distribution of redox-sensitive TMs directly over the shelf appears to have been propagated offshore (Figure 3 and Text S4). Within the offshore OMZ, Fe (II) was below the detection limit (<0.2 nM) on Transect 1 at stations 6 and 5, located 170 and 330 km offshore, respectively. In contrast, enhanced concentrations of 0.4–0.5 nM Fe (II) were present along Transects 2 and 3, and highest offshore Fe (II) concentrations of 4.2 and 4.6 nM were finally reached at station 17 of Transect 4 (depths of 148 and 322 m, respectively). Comparing offshore concentrations of dFe and reactive pFe within the OMZ at similar distances from the coast (130–170 km) showed the lowest concentrations along Transect 1 (dFe <1.3 nM; reactive pFe <5.7 nM; O_2 ~0 μM between 291- and 480-m depth) and the highest concentrations along Transect 4 (up to 2.8-nM dFe; 10.1 nM reactive pFe, O_2 ~0 μM between 93- and 440-m depth). This trend was matched by the redox-sensitive metals dCo and dMn (Figures 3i and 3j). In contrast, macronutrients and non-redox-sensitive TMs with nutrient-like behavior (phosphate, silicic acid, dCd, and dNi) showed less offshore variation between the transects (Figures 3e and 3k-3m). This indicates a much smaller influence of El Niño on macronutrient-like TMs and supports the influence of redox-related processes, such as sediment release and oxidative removal, being responsible for the observed variability in Fe, Co, and Mn distributions.

3.5. Potential Impacts on Phytoplankton Productivity

Bioassay experiments have demonstrated Fe-limited phytoplankton growth throughout the study region, including during our cruise occupation (Browning et al., 2018; Hutchins et al., 2002). The overall lower dFe in both surface and subsurface waters (in density layers that subsequently upwell; Figure 4), combined with higher ratios of nitrate + nitrite to dFe (Figures 2n and 3n; Browning et al., 2017) at onshore and offshore stations along Transect 1 compared to Transects 2–4, indicates that the more oxidizing water column conditions induced by the El Niño event would result in a faster off-shelf transition into Fe limiting conditions, possibly driving overall reductions in productivity (Bruland et al., 2005; Johnson et al., 1999). Indeed, postcruise reductions in satellite-derived chlorophyll-a concentrations relative to a climatological average were found for the Peruvian Shelf region (November/December 2015), possibly driven by sustained reductions in Fe supply to surface waters (Browning et al., 2018).

4. Conclusion

Our observations have demonstrated the critical control of seawater oxidation state, within the context of shelf width (Bruland et al., 2005; Johnson et al., 1999), on water column concentrations of redox-sensitive micronutrient metals in the Peruvian Upwelling zone. Specifically, oxygenation of waters of the North Peruvian shelf (>18 μM O_2) resulted in a tenfold decrease in dFe compared to the same location sampled in a previous study (Bruland et al., 2005). Such data are essential for evaluations of on-going changes in biogeochemistry and overall productivity of eastern boundary upwelling zones (Capone & Hutchins, 2013). In the future, OMZs are however proposed to be more, rather than less, oxygen-depleted, whereas El Niño events may become more frequent (Cai et al., 2018; Schmidtko et al., 2017). Intermittent oxic events in OMZs leading to Fe precipitation from the water column have been suggested to play a critical role in

resupplying Fe to sediments, which can subsequently be released following resumption of anoxia (Noffke et al., 2012; Scholz et al., 2011). Episodic oxygenation thus also requires consideration when evaluating the feedback of deoxygenation, Fe supply, phytoplankton productivity, and the associated network of interconnected biogeochemical cycles into the future.

5. Data Availability Statement

All trace metal and iodide/iodate data are freely available on PANGAEA (https://doi.pangaea.de/10.1594/PANGAEA.913798). Nutrient data are freely available on PANGEA (https://doi.pangaea.de/10.1594/PANGAEA.861391).

Acknowledgments
The authors thank the captain, crew and chief scientists, C.A. Marandino, T. Steinhoff, and D. Grundle of the RV Sonne SO243 cruise. M. Hopwood is thanked for useful discussions and advice for the Fe (II) measurements. We would like to thank the anonymous reviewers for detailed comments that improved the manuscript. This work was funded by the Deutsche Forschungsgemeinschaft as part of Sonderforschungsbereich (SFB) 754: "Climate-Biogeochemistry Interactions in the Tropical Ocean." T. J. B. was funded by a Marie Skłodowska-Curie Postdoctoral European Fellowship (OceanLiNES; grant 658035). The cruise was funded by the Bundesministerium für Bildung und Forschung (03G0243A). F. A. C. L. M. was funded by a DFG Fellowship of the Excellence Cluster "The Future Ocean" (TRANSFER; grant CP1403).

References

Biller, D. V., & Bruland, K. W. (2013). Sources and distributions of Mn, Fe, Co, Ni, Cu, Zn, and Cd relative to macronutrients along the central California coast during the spring and summer upwelling season. *Marine Chemistry*, *155*, 50–70. https://doi.org/10.1016/j.marchem.2013.06.003

Bonnet, S., Guieu, C., Bruyant, F., Prášil, O., van Wambeke, F., Raimbault, P., et al. (2008). Nutrient limitation of primary productivity in the Southeast Pacific (BIOSOPE cruise). *Biogeosciences*, *5*(1), 215–225. https://doi.org/10.5194/bg-5-215-2008

Boyd, P. W., & Ellwood, M. J. (2010). The biogeochemical cycle of iron in the ocean. *Nature Geoscience*, *3*(10), 675–682. https://doi.org/10.1038/ngeo964

Browning, T. J., Achterberg, E. P., Rapp, I., Engel, A., Bertrand, E. M., Tagliabue, A., & Moore, C. M. (2017). Nutrient co-limitation at the boundary of an oceanic gyre. *Nature*, *551*(7679), 242–246. https://doi.org/10.1038/nature24063

Browning, T. J., Rapp, I., Schlosser, C., Gledhill, M., Achterberg, E. P., Bracher, A., & Le Moigne, F. A. C. (2018). Influence of iron, cobalt, and vitamin B_{12} supply on phytoplankton growth in the tropical East Pacific during the 2015 El Niño. *Geophysical Research Letters*, *45*, 6150–6159. https://doi.org/10.1029/2018gl077972

Bruland, K. W., & Lohan, M. C. (2006). Controls of trace metals in seawater. In: The oceans and marine geochemistry. In H. Elderfield (Ed.), *Treatise on Geochemistry* (Vol. 6, chap. 6.02, pp. 23–47). Oxford: Elsevier. https://doi.org/10.1016/B0-08-043751-6/06105-3

Bruland, K. W., Rue, E. L., & Smith, G. J. (2001). Iron and macronutrients in California coastal upwelling regimes: Implications for diatom blooms. *Limnology and Oceanography*, *46*(7), 1661–1674. https://doi.org/10.4319/lo.2001.46.7.1661

Bruland, K. W., Rue, E. L., Smith, G. J., & DiTullio, G. R. (2005). Iron, macronutrients and diatom blooms in the Peru upwelling regime: Brown and blue waters of Peru. *Marine Chemistry*, *93*(2–4), 81–103. https://doi.org/10.1016/j.marchem.2004.06.011

Buck, C. S., Aguilar-Islas, A., Marsay, C., Kadko, D., & Landing, W. M. (2019). Trace element concentrations, elemental ratios, and enrichment factors observed in aerosol samples collected during the US GEOTRACES eastern Pacific Ocean transect (GP16). *Chemical Geology*, *511*, 212–224. https://doi.org/10.1016/j.chemgeo.2019.01.002

Burdige, D. J. (1993). The biogeochemistry of manganese and iron reduction in marine-sediments. *Earth-Science Reviews*, *35*(3), 249–284. https://doi.org/10.1016/0012-8252(93)90040-E

Cai, W., Wang, G., Dewitte, B., Wu, L., Santoso, A., Takahashi, K., et al. (2018). Increased variability of eastern Pacific El Niño under greenhouse warming. *Nature*, *564*(7735), 201–206. https://doi.org/10.1038/s41586-018-0776-9

Capone, D. G., & Hutchins, D. A. (2013). Microbial biogeochemistry of coastal upwelling regimes in a changing ocean. *Nature Geoscience*, *6*(9), 711–717. https://doi.org/10.1038/Ngeo1916

Carr, M.-E. (2001). Estimation of potential productivity in eastern boundary currents using remote sensing. *Deep Sea Research Part II: Topical Studies in Oceanography*, *49*(1), 59–80. https://doi.org/10.1016/S0967-0645(01)00094-7

Chaillou, G., Anschutz, P., Lavaux, G., Schafer, J., & Blanc, G. (2002). The distribution of Mo, U, and Cd in relation to major redox species in muddy sediments of the Bay of Biscay. *Marine Chemistry*, *80*(1), 41–59. https://doi.org/10.1016/S0304-4203(02)00097-X

Chapman, P., & Liss, P. S. (1977). Effect of nitrite on spectrophotometric determination of iodate in seawater. *Marine Chemistry*, *5*(3), 243–249. https://doi.org/10.1016/0304-4203(77)90019-6

Chever, F., Rouxel, O. J., Croot, P. L., Ponzevera, E., Wuttig, K., & Auro, M. (2015). Total dissolvable and dissolved iron isotopes in the water column of the Peru upwelling regime. *Geochimica et Cosmochimica Acta*, *162*, 66–82. https://doi.org/10.1016/j.gca.2015.04.031

Christensen, V., de la Puente, S., Sueiro, J. C., Steenbeek, J., & Majluf, P. (2014). Valuing seafood: The Peruvian fisheries sector. *Marine Policy*, *44*(supplement C), 302–311. https://doi.org/10.1016/j.marpol.2013.09.022

Cutter, G., Andersson, P., Codispoti, L., Croot, P., Francois, R., Lohan, M., et al. (2010). Sampling and sample-handling protocols for GEOTRACES Cruises: GEOTRACES.

Cutter, G. A., Moffett, J. G., Nielsdóttir, M. C., & Sanial, V. (2018). Multiple oxidation state trace elements in suboxic waters off Peru: In situ redox processes and advective/diffusive horizontal transport. *Marine Chemistry*, *201*, 77–89. https://doi.org/10.1016/j.marchem.2018.01.003

Froelich, P. N., Klinkhammer, G. P., Bender, M. L., Luedtke, N. A., Heath, G. R., Cullen, D., et al. (1979). Early oxidation of organic-matter in pelagic sediments of the eastern equatorial Atlantic-suboxic diagenesis. *Geochimica et Cosmochimica Acta*, *43*(7), 1075–1090. https://doi.org/10.1016/0016-7037(79)90095-4

Gledhill, M., & Buck, K. N. (2012). The organic complexation of iron in the marine environment: A review. *Frontiers in Microbiology*, *3*, 69. https://doi.org/10.3389/fmicb.2012.00069

Hawco, N. J., Ohnemus, D. C., Resing, J. A., Twining, B. S., & Saito, M. A. (2016). A dissolved cobalt plume in the oxygen minimum zone of the eastern tropical South Pacific. *Biogeosciences*, *13*, 5697–5717. https://doi.org/10.5194/bg-13-5697-2016

Heller, M. I., Lam, P. J., Moffett, J. W., Till, C. P., Lee, J. M., Toner, B. M., & Marcus, M. A. (2017). Accumulation of Fe oxyhydroxides in the Peruvian oxygen deficient zone implies non-oxygen dependent Fe oxidation. *Geochimica et Cosmochimica Acta*, *211*, 174–193. https://doi.org/10.1016/j.gca.2017.05.019

Homoky, W. B., Weber, T., Berelson, W. M., Conway, T. M., Henderson, G. M., van Hulten, M., et al. (2016). Quantifying trace element and isotope fluxes at the ocean-sediment boundary: A review. *Philosophical Transactions of the Royal Society a-Mathematical Physical and Engineering Sciences*, *374*(2081), 20,160,246. https://doi.org/10.1098/rsta.2016.0246

Hopwood, M. J., Rapp, I., Schlosser, C., & Achterberg, E. P. (2017). Hydrogen peroxide in deep waters from the Mediterranean Sea, South Atlantic and South Pacific oceans. *Scientific Reports*, *7*(1), 1–10. https://doi.org/10.1038/srep43436

Hutchins, D. A., Hare, C. E., Weaver, R. S., Zhang, Y., Firme, G. F., DiTullio, G. R., et al. (2002). Phytoplankton iron limitation in the Humboldt current and Peru upwelling. *Limnology and Oceanography*, *47*(4), 997–1011. https://doi.org/10.4319/lo.2002.47.4.0997

Johnson, K. S., Chavez, F. P., & Friederich, G. E. (1999). Continental-shelf sediment as a primary source of iron for coastal phytoplankton. *Nature*, *398*(6729), 697–700. https://doi.org/10.1038/19511

Kagaya, S., Maeba, E., Inoue, Y., Kamichatani, W., Kajiwara, T., Yanai, H., et al. (2009). A solid phase extraction using a chelate resin immobilizing carboxymethylated pentaethylenehexamine for separation and preconcentration of trace elements in water samples. *Talanta*, *79*(2), 146–152. https://doi.org/10.1016/j.talanta.2009.03.016

Karstensen, J., Stramma, L., & Visbeck, M. (2008). Oxygen minimum zones in the eastern tropical Atlantic and Pacific oceans. *Progress in Oceanography*, *77*(4), 331–350. https://doi.org/10.1016/j.pocean.2007.05.009

Klinkhammer, G., Heggie, D. T., & Graham, D. W. (1982). Metal diagenesis in oxic marine sediments. *Earth and Planetary Science Letters*, *61*(2), 211–219. https://doi.org/10.1016/0012-879821X(82)90054-1

Lam, P. J., Ohnemus, D. C., & Marcus, M. A. (2012). The speciation of marine particulate iron adjacent to active and passive continental margins. *Geochimica et Cosmochimica Acta*, *80*, 108–124. https://doi.org/10.1016/j.gca.2011.11.044

Lohan, M. C., & Bruland, K. W. (2008). Elevated Fe (II) and dissolved Fe in hypoxic shelf waters off Oregon and Washington: An enhanced source of iron to coastal upwelling regimes. *Environmental Science & Technology*, *42*(17), 6462–6468. https://doi.org/10.1021/es800144j

Luther, G. W., Swartz, C. B., & Ullman, W. J. (1988). Direct determination of iodide in seawater by cathodic stripping square-wave voltammetry. *Analytical Chemistry*, *60*(17), 1721–1724. https://doi.org/10.1021/ac00168a017

Millero, F. J., Sotolongo, S., & Izaguirre, M. (1987). The oxidation kinetics of Fe (II) in seawater. *Geochimica et Cosmochimica Acta*, *51*(4), 793–801. https://doi.org/10.1016/0016-7037(87)90093-7

Moore, C. M., Mills, M. M., Arrigo, K. R., Berman-Frank, I., Bopp, L., Boyd, P. W., et al. (2013). Processes and patterns of oceanic nutrient limitation. *Nature Geoscience*, *6*(9), 701–710. https://doi.org/10.1038/Ngeo1765

Näykki, T., Virtanen, A., Kaukonen, L., Magnusson, B., Vaisanen, T., & Leito, I. (2015). Application of the nordtest method for "real-time" uncertainty estimation of on-line field measurement. *Environmental Monitoring and Assessment*, *187*(10), 1–12. https://doi.org/10.1007/s10661-015-4856-0

National Oceanic and Atmospheric Administration. (2017). Historical El Niño/La Niña episodes (150-present). From NOAA Centre for Weather and Climate Prediction. http://origin.cpc.ncep.noaa.gov/products/analysis_monitoring/ensostuff/ONI_v5.php

Noble, A. E., Lamborg, C. H., Ohnemus, D. C., Lam, P. J., Goepfert, T. J., Measures, C. I., et al. (2012). Basin-scale inputs of cobalt, iron, and manganese from the Benguela-Angola front to the South Atlantic Ocean. *Limnology and Oceanography*, *57*(4), 989–1010. https://doi.org/10.4319/lo.2012.57.4.0989

Noffke, A., Hensen, C., Sommer, S., Scholz, F., Bohlen, L., Mosch, T., et al. (2012). Benthic iron and phosphorus fluxes across the Peruvian oxygen minimum zone. *Limnology and Oceanography*, *57*(3), 851–867. https://doi.org/10.4319/lo.2012.57.3.0851

Pakhomova, S. V., Hall, P. O., Kononets, M. Y., Rozanov, A. G., Tengberg, A., & Vershinin, A. V. (2007). Fluxes of iron and manganese across the sediment–water interface under various redox conditions. *Marine Chemistry*, *107*(3), 319–331. https://doi.org/10.1016/j.marchem.2007.06.001

Pauly, D., & Christensen, V. (1995). Primary production required to sustain global fisheries. *Nature*, *374*, 255–257.

Plass, A., Schlosser, C., Sommer, S., Dale, A. W., Achterberg, E. P., & Scholz, F. (2019). The control of hydrogen sulfide on benthic iron and cadmium fluxes in the oxygen minimum zone off Peru. *Biogeosciences Discussions*. https://doi.org/10.5194/bg-2019-390 in review

Rapp, I., Schlosser, C., Menzel Barraqueta, J.-L., Wenzel, B., Lüdke, J., Scholten, J., et al. (2019). Controls on redox-sensitive trace metals in the Mauritanian oxygen minimum zone. *Biogeosciences*, *16*(21), 4157–4182. https://doi.org/10.5194/bg-16-4157-2019

Rapp, I., Schlosser, C., Rusiecka, D., Gledhill, M., & Achterberg, E. P. (2017). Automated preconcentration of Fe, Zn, Cu, Ni, Cd, Pb, Co, and Mn in seawater with analysis using high-resolution sector field inductively-coupled plasma mass spectrometry. *Analytica Chimica Acta*, *976*, 1–13. https://doi.org/10.1016/j.aca.2017.05.008

Sanial, V., Kipp, L. E., Henderson, P. B., van Beek, P., Reyss, J. L., Hammond, D. E., et al. (2018). Radium-228 as a tracer of dissolved trace element inputs from the Peruvian continental margin. *Marine Chemistry*, *201*, 20–34. https://doi.org/10.1016/j.marchem.2017.05.008

Schlosser, C., Streu, P., Frank, M., Lavik, G., Croot, P. L., Dengler, M., & Achterberg, E. P. (2018). H_2S events in the Peruvian oxygen minimum zone facilitate enhanced dissolved Fe concentrations. *Scientific Reports*, *8*. https://doi.org/10.1038/s41598-018-30580-w

Schmidtko, S., Stramma, L., & Visbeck, M. (2017). Decline in global oceanic oxygen content during the past five decades. *Nature*, *542*(7641), 335–339. https://doi.org/10.1038/nature21399

Scholz, F., Hensen, C., Noffke, A., Rohde, A., Liebetrau, V., & Wallmann, K. (2011). Early diagenesis of redox-sensitive trace metals in the Peru upwelling area—Response to ENSO-related oxygen fluctuations in the water column. *Geochimica et Cosmochimica Acta*, *75*(22), 7257–7276. https://doi.org/10.1016/j.gca.2011.08.007

Scholz, F., Löscher, C. R., Fiskal, A., Sommer, S., Hensen, C., Lomnitz, U., et al. (2016). Nitrate-dependent iron oxidation limits iron transport in anoxic ocean regions. *Earth and Planetary Science Letters*, *454*, 272–281. https://doi.org/10.1016/j.epsl.2016.09.025

Severmann, S., McManus, J., Berelson, W. M., & Hammond, D. E. (2010). The continental shelf benthic iron flux and its isotope composition. *Geochimica et Cosmochimica Acta*, *74*(14), 3984–4004. https://doi.org/10.1016/j.gca.2010.04.022

Stramma, L., Fischer, T., Grundle, D. S., Krahmann, G., Bange, H. W., & Marandino, C. A. (2016). Observed El Niño conditions in the eastern tropical Pacific in October 2015. *Ocean Science*, *12*(4), 861–873. https://doi.org/10.5194/os-12-861-2016

Sunda, W. G., & Huntsman, S. A. (1994). Photoreduction of manganese oxides in seawater. *Marine Chemistry*, *46*(1–2), 133–152. https://doi.org/10.1016/0304-4203(94)90051-5

Vedamati, J., Goepfert, T., & Moffett, J. W. (2014). Iron speciation in the eastern tropical South Pacific oxygen minimum zone off Peru. *Limnology and Oceanography*, *59*(6), 1945–1957. https://doi.org/10.4319/lo.2014.59.6.1945

Ward, B. A., Dutkiewicz, S., Moore, C. M., & Follows, M. J. (2013). Iron, phosphorus, and nitrogen supply ratios define the biogeography of nitrogen fixation. *Limnology and Oceanography*, *58*(6), 2059–2075. https://doi.org/10.4319/lo.2013.58.6.2059

Wong, G. T. F., & Brewer, P. G. (1977). Marine chemistry of iodine in anoxic basins. *Geochimica et Cosmochimica Acta*, *41*(1), 151–159. https://doi.org/10.1016/0016-7037(77)90195-8

Wong, G. T. F., Piumsomboon, A. U., & Dunstan, W. M. (2002). The transformation of iodate to iodide in marine phytoplankton cultures. *Marine Ecology Progress Series*, *237*, 27–39. https://doi.org/10.3354/meps237027